Designing Low-Thrust Transfers to High-Inclination Science Orbits via Hybrid Optimization

Christopher J. Sullivan*
University of Colorado Boulder, Boulder, CO 80303

Jeffrey Stuart† and Rodney L. Anderson†
Jet Propulsion Laboratory, California Institute of Technology, Pasadena, CA 91109

Natasha Bosanac‡
University of Colorado Boulder, Boulder, CO 80303

Placing a small satellite into a high-inclination orbit with respect to the ecliptic plane may offer a low-cost option for opportunistic and targeted observations of the polar regions of the Sun or the zodiacal dust cloud of our solar system. In this paper, dynamical systems theory and hybrid optimization techniques are integrated into a cohesive framework to design low-thrust trajectories for a small satellite to reach a highly out-of-ecliptic science orbit near the Sun-Earth L_2 equilibrium point. Propellant-optimal, low-thrust trajectories with a specific geometry are designed and studied across a variety of engine and power models within a low-thrust-enabled circular restricted three-body problem. The geometry of the trajectories is then varied during the initial guess construction process to support a preliminary study of the trade-off between flight time and propellant mass usage.

Nomenclature

C_J	=	Jacobi constant
$\boldsymbol{d}_i$	=	position vector measured from primary body i to spacecraft
d_i	=	spacecraft distance to primary body i
$\boldsymbol{F}$	=	constraint vector
$\boldsymbol{f}_n$	=	acceleration vector associated with natural dynamics
$\tilde{g}_0$	=	gravitational acceleration measured at the surface of Earth, m/s^2
H	=	Hamiltonian
$\tilde{I}_{sp}$	=	engine specific impulse, s
J	=	objective function

*Ph.D. Student, Ann and H.J. Smead Aerospace Engineering Sciences, 3775 Discovery Dr., Student Member AIAA.
†Technologist, Mission Design & Navigation, Member AIAA.
‡Assistant Professor, Ann and H.J. Smead Aerospace Engineering Sciences, Member AIAA.

This version of the paper has been accepted for publication by AIAA's Journal of Spacecraft and Rockets after peer review but does not reflect any changes due to copy-editing and formatting by AIAA. The published manuscript is available online at: https://arc.aiaa.org/doi/full/10.2514/1.A34980

L:i-A:j-V:k	=	transfer constructed from i L_2 Lyapunov orbits, j L_2 axial orbits, and k L_2 vertical orbits
l^*	=	characteristic distance, km
m	=	spacecraft mass
n	=	number of arcs
$\boldsymbol{N}$	=	subvector of free variables along an arc
P	=	engine power in nondimensional units
$\tilde{P}$	=	engine power in dimensional units, W
$\boldsymbol{r}$	=	position vector
$\boldsymbol{s}$	=	state vector without mass
T	=	engine thrust in nondimensional units
$\tilde{T}$	=	engine thrust in dimensional units, N
t^*	=	characteristic time, s
TD	=	integration time constraint
U	=	constraint on thrust direction unit vector magnitude
$\boldsymbol{u}$	=	thrust direction unit vector
$\boldsymbol{v}$	=	velocity vector
$\boldsymbol{X}$	=	free variable vector
$\boldsymbol{x}$	=	state vector with mass
β_i	=	slack variable
Δm	=	discontinuity in spacecraft mass
Δt	=	propagation time
$\boldsymbol{\nu}$	=	vector of Lagrange multipliers
$\boldsymbol{\lambda}$	=	co-state vector
μ	=	mass ratio
τ	=	time along periodic orbit
$\boldsymbol{\psi}$	=	boundary condition vector

Subscripts

C	=	coast arc
D	=	departure
f	=	final
L	=	thrust arc
ℓ	=	neighboring low-thrust arcs

max	=	maximum value
0	=	initial
ref	=	reference value
T	=	target

I. Introduction

Trajectories that deliver small spacecraft to mission orbits that extend well beyond the ecliptic plane are enabling for various mission concepts in heliophysics and astronomy. Excursions of even 15° out of the ecliptic plane may supply an external view of the three-dimensional structure of the zodiacal dust cloud, with implications for solar system evolution and exoplanetary surveys [1, 2]. These vantage points also offer a line of sight to the poles of the Sun, previously observed by the Ulysses spacecraft and soon to be observed by the Solar Orbiter spacecraft, which launched in February 2020 [3, 4]. With recent advancements in spacecraft technology, spacecraft tailored to a SmallSat form factor may soon be launched as secondary payloads or on small launch vehicles to provide low-cost and targeted space-based observations of these phenomena [5]. Once deployed, a SmallSat that is equipped with a propulsion system may perform maneuvers to access a variety of science orbits, widening the scope for mission concept development [5–8].

In this paper, propellant-optimal trajectories are designed for a SmallSat that is equipped with a high efficiency, low-thrust propulsion system with the goal of enabling missions to science orbits with significant out-of-ecliptic excursions. This SmallSat is assumed to be compatible with an Evolved Expendable Launch Vehicle Secondary Payload Adapter (ESPA). Although there may be various, suitable high-inclination mission orbits relative to the ecliptic plane, this analysis focuses specifically on Sun-Earth L_2 vertical orbits as a target. These orbits exist in the circular restricted three-body problem (CR3BP) and are approximately retained in high-fidelity models of the Sun-Earth system. It is also assumed that a Sun-Earth L_2 Lyapunov orbit is accessible from a variety of deployment conditions associated with upcoming rideshare opportunities [5–7]. Under these assumptions, this paper focuses on designing propellant-optimal low-thrust trajectories for a SmallSat to reach an L_2 vertical orbit from an L_2 Lyapunov orbit in the Sun-Earth system. To enable a rapid and informed design procedure, an initial guess is constructed in the CR3BP using techniques derived from dynamical systems theory and then input to a hybrid optimization scheme to recover a nearby continuous trajectory.

Researchers throughout the astrodynamics community have demonstrated the capability for dynamical systems theory to rapidly generate an initial guess for a low-thrust trajectory in a multi-body system. Early observations of the low-thrust solutions obtained using the Mystic optimization software note a resemblance to the hyperbolic invariant manifolds of unstable periodic orbits in the CR3BP [9–12]. Anderson and Lo also demonstrated that optimal trajectories for tour design using the Jovian moons closely follow the hyperbolic invariant manifolds of unstable resonant periodic orbits [13]. However, due to the complexity of analyzing spatial hyperbolic invariant manifolds, an alternative approach, which is employed in this paper, has also emerged within the community: using arcs along periodic orbits to construct an initial guess for a low-thrust trajectory. Parker and Anderson, Pritchett, Zimovan, and Howell, and Das-Stuart, Howell, and Folta, for example, demonstrate this process for incorporating periodic orbit families into the transfer design process in both the CR3BP and higher fidelity models [14–16]. Using these results as a foundation, periodic orbits in the vicinity of Sun-Earth L_2 are used in this paper to seed an initial guess for a low-thrust trajectory with a desired itinerary. In addition, distinct sequences of periodic orbits are used to seed initial guesses of various geometries. These initial guesses are then used to recover a continuous trajectory via corrections and optimization.

In general, the computation of locally fuel-optimal trajectories is posed as an optimal control problem that is solved using a combination of indirect and direct methods. Indirect techniques offer a low-dimensional yet numerically sensitive approach using optimal control theory while direct methods offer a higher-dimensional but more robust approach [17–21]. A combination of an indirect and a direct method is termed a hybrid optimization algorithm and exploits the benefits of both optimization strategies. In this paper, the Euler-Lagrange theorem offers conditions for optimal engine operation, while either the commercial optimization package SNOPT or the function *fmincon* in MATLAB© are used to recover a feasible and propellant-optimal low-thrust trajectory [22–24].

The assumed propulsion system model significantly influences the complexity of generating low-thrust transfers between the selected orbits. Propellant-optimal, low-thrust trajectories realized by Constant Specific Impulse (CSI) systems in multi-body regimes typically require coasting arcs and the careful balancing of engine capability with transfer time. However, a Variable Specific Impulse (VSI) engine that varies the thrust magnitude simplifies the generation of transfer solutions [25, 26]. In addition, two models of the power supplied to the low-thrust engine are employed: 1) a constant power approximation that enables the rapid recovery of a locally-optimal low-thrust trajectory and 2) a higher-fidelity varying power model that depends on the distance of the spacecraft from the Sun. To generate comparable trajectories in each of these engine and power models, a continuation-based approach is employed: a trajectory recovered for one engine and power model is used to seed an initial guess for the trajectory in a higher-fidelity engine and/or power model. This continuation-based approach reduces the required computational effort and sensitivity associated with recovering a low-thrust trajectory that resembles an initial guess designed using dynamical systems theory [27].

In this paper, low-thrust transfers from a Sun-Earth L_2 Lyapunov orbit to a Sun-Earth L_2 vertical orbit are explored. First, one initial guess is constructed using a specific sequence of Lyapunov, axial, and vertical orbits near Sun-Earth L_2. This discontinuous initial guess is used to generate a propellant-optimal and continuous-thrust trajectory for a constant power VSI engine; the result is a trajectory that requires 11.80 years of flight time and 43.26 kg of propellant for a SmallSat with an initial wet mass of 180 kg and a reference engine power of 90 W at 1 AU. This solution is then used to seed an initial guess for a continuous-thrust transfer for a varying power VSI engine. The same initial guess is also used to construct trajectories that combine natural and low-thrust-enabled motion for a constant power VSI engine and a CSI engine. In these scenarios, the coast arcs are placed at scientifically valuable locations coinciding with the regions of lowest thrust along the continuous-thrust VSI transfers used to seed the initial guess. The properties of these solutions across each of the propulsion system models are studied. Then, variations in the sequence of intermediate orbits are used to influence the resulting locally optimal transfer and study the solution space, with a focus on the flight time and propellant mass usage; this solution space is composed of continuous-thrust transfers and trajectories that leverage both natural and low-thrust arcs. Solutions are identified with a minimum flight time of five years and high propellant mass requirement, while longer transfers require a minimum of approximately 40 kg of propellant mass for the assumed spacecraft form factor. Based on these results, this paper offers two contributions: i) a framework for designing low-thrust trajectories for a SmallSat to reach a high-inclination orbit near Sun-Earth L_2 for engine and power models of various fidelity; and, ii) a preliminary exploration of the trade between propellant mass usage and flight time across the recovered solution space. These contributions may support the recovery of the trajectory design space during mission concept development in a similar scenario as the SmallSat configuration or mission parameters evolve; with a specific set of hardware parameters, path and operational constraints, and mission requirements, these solutions may enable future analysis of the existence and properties of feasible transfers.

II. Background: Dynamical and Spacecraft Models

The CR3BP is leveraged as a fundamental model of the natural dynamics governing a spacecraft under the gravitational influence of both the Sun and Earth. In this dynamical model, two primaries, the Sun and Earth, are assumed to travel along circular orbits around their mutual barycenter [28]. In addition, the mass of the spacecraft is assumed to be negligible in comparison. Under these assumptions, the CR3BP is formulated using a rotating reference frame $\hat{x}\hat{y}\hat{z}$: $\hat{x}$ is directed from the Sun to Earth, $\hat{z}$ is aligned with the orbital angular momentum of the primaries, and $\hat{y}$ completes the right-handed set. Then, length and time quantities are nondimensionalized using $l^* = 1.4960 \times 10^8$ km and $t^* = 5.0230 \times 10^6$ s; mass quantities are nondimensionalized to produce a mass ratio of $\mu = 3.0039 \times 10^{-6}$ in the Sun-Earth system [29]. Parameters that are not normalized by any of these characteristics quantities are denoted throughout the text by using the tilde notation. Using these definitions, the nondimensional state of the spacecraft in the natural CR3BP is expressed in the rotating frame and relative to the barycenter of the Sun-Earth system via the position vector $\boldsymbol{r} = [x, y, z]^T$ and the velocity vector $\boldsymbol{v} = [\dot{x}, \dot{y}, \dot{z}]^T$. Then, the acceleration vector $\boldsymbol{f}_n$ of the spacecraft in the natural CR3BP is written in the rotating frame as

$$\boldsymbol{f}_n = \begin{bmatrix} 2\dot{y} + x - \frac{(1-\mu)(x+\mu)}{d_1^3} - \frac{\mu(x-1+\mu)}{d_2^3} \\ -2\dot{x} + y - \frac{(1-\mu)y}{d_1^3} - \frac{\mu y}{d_2^3} \\ -\frac{(1-\mu)z}{d_1^3} - \frac{\mu z}{d_2^3} \end{bmatrix} \tag{1}$$

where $d_1 = \sqrt{(x+\mu)^2 + y^2 + z^2}$ and $d_2 = \sqrt{(x-1+\mu)^2 + y^2 + z^2}$ [28]. The CR3BP admits an integral of motion labeled the Jacobi constant, equal to $C_J = (x^2+y^2) + \frac{2(1-\mu)}{d_1} + \frac{2\mu}{d_2} - \dot{x}^2 - \dot{y}^2 - \dot{z}^2$ [28]. This energy-like quantity offers valuable insight in both the CR3BP and under perturbations when developing heuristics for trajectory design [6, 7].

When the low-thrust engine is activated, the spacecraft applies an additional acceleration that depends on the engine thrust and power model. In this paper, two fundamental engine models are employed. First, a CSI engine is modeled by assuming that both the thrust magnitude $\tilde{T}$ and available power $\tilde{P}$ are constants [5]. A VSI engine, however, considers a variable thrust magnitude over time. For the VSI engine model, two available power models are employed: a constant power approximation and a varying power level that depends on the distance of the spacecraft from the Sun. In each case, the power $\tilde{P}$ is a positive scalar quantity that is constrained at or below a maximum available power $\tilde{P}_{\max}$ that is defined in terms of the reference power $\tilde{P}_{\text{ref}}$, the power available to the solar electric propulsion (SEP) system at 1 AU. For a constant power approximation, the maximum available power to the engine is set equal to the reference power, i.e., $\tilde{P}_{\max} = \tilde{P}_{\text{ref}}$. However, for a varying power model, the maximum available power is equal to $\tilde{P}_{\max} = \tilde{P}_{\text{ref}}/d_1^2$. For each of these engine and power models, the specific impulse is calculated from the thrust magnitude and power as $\tilde{I}_{sp} = 2\tilde{P}/(\tilde{T}\tilde{g}_0)$. In this paper, the spacecraft and engine properties are derived consistent with the ESPA-class SmallSat platform and using two Jet Propulsion Laboratory (JPL) Miniature Xenon Ion (MiXI) thrusters at the theoretical maximum thrust level to model a CSI engine [30]. The defined parameter values are summarized in Table 1. Note that the thrust magnitude and specific impulse for a VSI engine are unconstrained and calculated using optimization [27]; they are both calculated along each trajectory and compared to the nominal values for the CSI engine.

The equations of motion for the natural CR3BP are modified to incorporate the acceleration induced by a low-thrust engine. First, the state vector is redefined as $\boldsymbol{x} = [x, y, z, \dot{x}, \dot{y}, \dot{z}, m]^T$ to include m, the instantaneous spacecraft mass normalized by the initial wet mass $\tilde{m}_0$. When the low-thrust engine is activated, the normalized spacecraft mass is reduced at a rate $\dot{m}$ that is nondimensionalized by the characteristic time and initial wet mass of the spacecraft. Then, the equations of motion for the low-thrust-enabled CR3BP are written in the rotating frame as

$$\dot{\boldsymbol{x}} = \begin{bmatrix} \dot{\boldsymbol{r}} \\ \dot{\boldsymbol{v}} \\ \dot{m} \end{bmatrix} = \begin{bmatrix} \boldsymbol{v} \\ \boldsymbol{f}_n(\boldsymbol{r}, \boldsymbol{v}) + \frac{T}{m}\boldsymbol{u} \\ -\frac{T^2}{2P} \end{bmatrix} \tag{2}$$

where T and P are the thrust magnitude and spacecraft power normalized using l^*, t^* and $\tilde{m}_0$ [31].

III. Technical Approach: Initial Guess Construction

An initial guess for a low-thrust trajectory is designed for an ESPA-class SmallSat to reach a highly out-of-ecliptic orbit from a planar libration point orbit while maximizing the final spacecraft mass. In this section, the departure and

Table 1 Low-thrust-enabled SmallSat parameters

Quantity	Value
SmallSat initial wet mass ($\tilde{m}_0$), kg	180
Reference power ($\tilde{P}_{\text{ref}}$) at 1 AU, W	90
CSI thrust ($\tilde{T}$), N	0.006
CSI specific impulse ($\tilde{I}_{sp}$), s	3000

arrival orbits are defined using periodic orbits in the Sun-Earth L_2 region. Then, dynamical systems techniques are employed to construct an initial guess for a low-thrust trajectory between these two orbits. An initial guess is constructed by assembling arcs along known periodic orbits in the CR3BP near Sun-Earth L_2; these periodic orbits are selected using fundamental insights into the structure of orbit families near Sun-Earth L_2 to ensure incremental changes in inclination and Jacobi constant. Given the low acceleration supplied by a miniaturized low-thrust engine, this approach enables recovery of a continuous low-thrust trajectory with similar characteristics to the constructed initial guess.

A. Reference Periodic Orbits

The well-known L_2 Lyapunov, axial, and vertical orbit families in the Sun-Earth CR3BP are leveraged in this paper for both mission orbit selection and initial guess construction. Selected members along each family in the Sun-Earth CR3BP are depicted in Fig. 1 in the rotating frame for the (a) L_2 Lyapunov, (b) L_2 axial, and (c) L_2 vertical orbit families. In this figure, each orbit is colored by the value of the Jacobi constant. Using this figure as a reference, members of the L_2 Lyapunov family encircle the L_2 libration point entirely within the xy-plane of the rotating frame; as the orbits grow larger across the family, C_J decreases. The L_2 vertical orbits follow a path that resembles a three-dimensional figure eight; as the orbits grow in size, the maximum inclination increases and the Jacobi constant decreases. In addition, the L_2 Lyapunov and vertical orbit families are connected via bifurcations with the L_2 axial family [32].

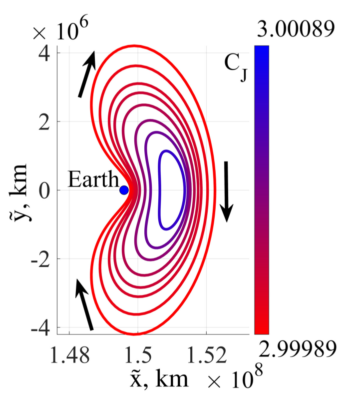

(a) L_2 Lyapunov family

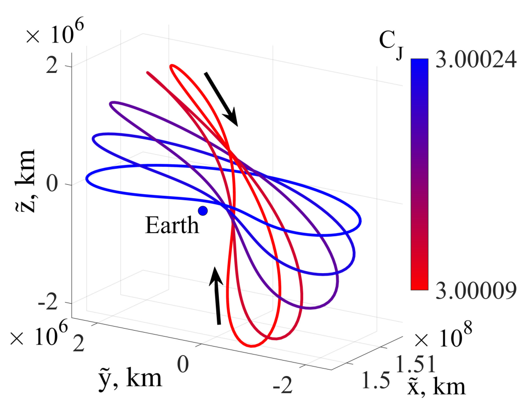

(b) L_2 axial family

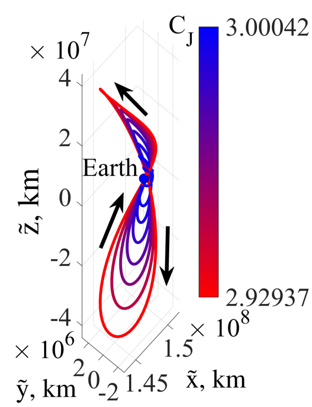

(c) L_2 vertical family

Fig. 1 Periodic orbit families near the Sun-Earth L_2 equilibrium point.

B. Departure and Arrival Orbits

Departure and arrival orbits are selected using periodic orbits in the Sun-Earth CR3BP. First, an L_2 Lyapunov orbit described by a Jacobi constant of 3.00050 is selected as the departure orbit in this paper due to the potential for accessibility from a variety of Earth-escape deployment conditions [5–7]. Then, recall that the goal of this work is to design a transfer for a SmallSat to be inserted into an orbit that regularly exhibits a large excursion out of the ecliptic plane. Members of the heliophysics community note that a mission orbit with a maximum inclination of at least 15° relative to the ecliptic plane may support useful out-of-plane observations and zodiacal dust measurements [1, 2]. The vertical family near Sun-Earth L_2 offers solutions where a spacecraft may spend a large fraction of time above or below the ecliptic plane to support long periods of scientific observations. Accordingly, a member of the L_2 vertical family with a 15.24° maximum inclination, measured from the Sun and with respect to the ecliptic plane, and a Jacobi constant of 2.92937 is selected as the target scientific orbit. These two orbits possess significant differences in inclination and Jacobi constant, motivating the use of a low-thrust engine along the transfer.

C. Constructing Initial Guesses via Orbit Sequences

An initial guess for a low-thrust transfer between the selected low-inclination Lyapunov and high-inclination vertical orbits is constructed using a sequence of periodic orbits within the Sun-Earth system. In this work, orbits selected along the L_2 axial family act as transitional segments to induce out-of-plane motion prior to reaching the vicinity of the L_2 vertical family in the phase space. Then, vertical orbits are used to gradually increase the inclination and energy. For a transfer labeled **L:i-A:j-V:k**, the initial guess is formed by assembling the following orbits in order of decreasing C_J:

- **L:i** - the initial L_2 Lyapunov orbit as well as $(i - 1)$ additional L_2 Lyapunov orbits selected at equally spaced values of the Jacobi constant between the starting orbit and the bifurcation with the L_2 axial family;
- **A:j** - j distinct L_2 axial orbits with Jacobi constants equally spaced between the bifurcations of the L_2 axial family with the L_2 Lyapunov and L_2 vertical families;
- **V:k** - $(k - 1)$ intermediate L_2 vertical orbits at equally spaced values of the Jacobi constant between the values of the Jacobi constant at the bifurcation of the L_2 vertical family with the L_2 axial family and the Jacobi constant of the selected target periodic orbit, followed by the target L_2 vertical orbit.

As an example, an initial guess for a **L:2-A:2-V:11** transfer is portrayed in Fig. 2 with: (a) a complete view of the trajectory in the Sun-Earth rotating frame and (b) a zoomed in view of the beginning of the transfer. In these figures, the black, dotted arc indicates the initial periodic orbit, the intermediate orbits are plotted in shades of purple and gold that reflect their ordering within the initial guess, and the final periodic orbit is represented in solid black. Through this initial guess construction approach, the optimization algorithm is biased towards a low-thrust trajectory that effectively leverages the natural dynamics in the Sun-Earth system. However, the number of initial guess orbits that are selected from the Sun-Earth L_2 periodic orbit families strongly influences the resulting locally optimal solution that is recovered.

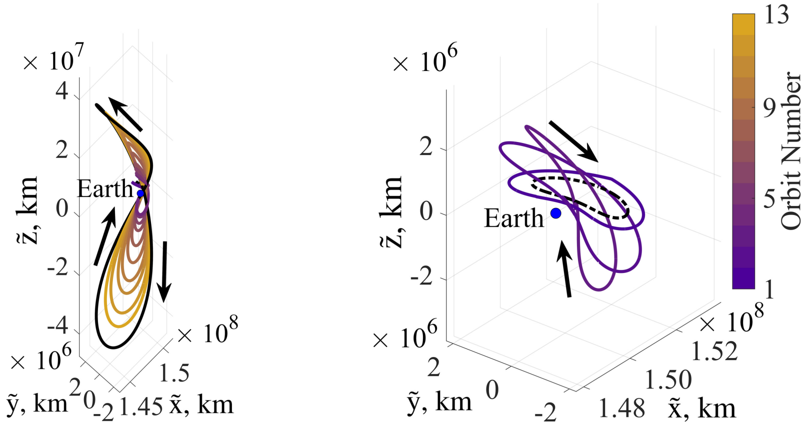

(a) (b)

Fig. 2 Initial guess for a L:2-A:2-V:11 transfer: (a) spatial view and (b) Lyapunov and axial segments.

Thus, a variety of initial guesses are constructed and labeled using the presented convention.

IV. Technical Approach: Hybrid Approach to Trajectory Optimization

A hybrid optimization strategy that combines indirect and direct optimization methods is used to recover locally optimal trajectories, subject to boundary and path constraints. Indirect optimization leverages calculus of variations to define a two-point boundary value problem (2PBVP) and recover the optimality conditions [33]. Direct methods, however, focus on the use of nonlinear programming to solve the optimal control problem [33]. In a hybrid optimization strategy, indirect procedures are combined with direct methods to retain low-dimensionality while increasing the robustness of the convergence process [33]. First, insights from calculus of variations are used to define optimal engine operation and determine the values of the control parameters along a trajectory. Then, gradient-based optimization is combined with a multiple shooting method using, for example, either SNOPT or *fmincon* in MATLAB to recover a feasible transfer between the departure and arrival periodic orbits while maximizing the final spacecraft mass [23, 24].

A. Indirect Optimization

An optimization problem is defined to recover low-thrust trajectories that maximize the final spacecraft mass subject to both boundary and system constraints. Maximizing the final spacecraft mass is equivalent to minimizing the propellant mass usage. When a VSI engine model is employed and the thrust duration is unconstrained, minimization of this objective function would drive the values of the thrust duration and the specific impulse to infinity; a result that is not feasible. Thus, the optimization problem is formulated in this paper for a fixed transfer time. The transfer is also subject to boundary conditions corresponding to the spacecraft departing from a specified initial periodic orbit and arriving into a final periodic orbit. These departure and arrival locations are defined using state vectors $\boldsymbol{s}_D(\tau_D)$ and $\boldsymbol{s}_T(\tau_T)$ along each of the departure and target periodic orbits, respectively, where $\boldsymbol{s} = [x, y, z, \dot{x}, \dot{y}, \dot{z}]^T$. Each of these state vectors is generated by propagating a specified initial condition along the periodic orbit for a time τ_D or τ_T, respectively. The boundary conditions are then written mathematically as

$$\boldsymbol{\psi}_0 = \boldsymbol{s}(t_0) - \boldsymbol{s}_D(\tau_D) = \boldsymbol{0} \qquad\qquad \boldsymbol{\psi}_f = \boldsymbol{s}(t_f) - \boldsymbol{s}_T(\tau_T) = \boldsymbol{0} \tag{3}$$

where $\boldsymbol{s}(t_0)$ and $\boldsymbol{s}(t_f)$ correspond to states at the initial and final times, respectively, along the transfer. The boundary conditions and system dynamics are then used to write the constrained optimization problem in Bolza form as

$$\max\left(J = m_f + \boldsymbol{\nu}_0^T \boldsymbol{\psi}_0 + \boldsymbol{\nu}_f^T \boldsymbol{\psi}_f + \int_{t_0}^{t_f} [H - \boldsymbol{\lambda}^T \dot{\boldsymbol{x}}] dt\right) \tag{4}$$

The co-state vector possesses the components $\boldsymbol{\lambda} = [\boldsymbol{\lambda}_{\boldsymbol{r}}^T, \boldsymbol{\lambda}_{\boldsymbol{v}}^T, \lambda_m]^T$ where $\boldsymbol{\lambda}_{\boldsymbol{r}}$ and $\boldsymbol{\lambda}_{\boldsymbol{v}}$ are three-dimensional vectors for the position and velocity co-states, respectively, and the scalar λ_m is the mass co-state [27].

The differential equations for the co-states are defined by formulating a 2PBVP using the calculus of variations. First, the Hamiltonian H is written in the low-thrust-enabled CR3BP as

$$H = \boldsymbol{\lambda}^T \dot{\boldsymbol{x}} = \boldsymbol{\lambda}_{\boldsymbol{r}}^T \boldsymbol{v} + \boldsymbol{\lambda}_{\boldsymbol{v}}^T \left[\boldsymbol{f}_n(t, \boldsymbol{r}, \boldsymbol{v}) + \frac{T}{m}\boldsymbol{u}\right] - \lambda_m \frac{T^2}{2P} \tag{5}$$

Using the Euler-Lagrange theorem and Pontryagin's maximization principle, this Hamiltonian is maximized with respect to each of the controls, i.e., T, P, and $\boldsymbol{u}$. The resulting optimal control strategy is summarized as

$$P = P_{\max} \qquad\qquad T = \frac{\lambda_{\boldsymbol{v}} P}{\lambda_m m} \qquad\qquad \boldsymbol{u} = \frac{\boldsymbol{\lambda}_{\boldsymbol{v}}}{||\boldsymbol{\lambda}_{\boldsymbol{v}}||} \tag{6}$$

where the spacecraft is operating at the maximum available power level and the final condition is consistent with primer vector theory [27]. When the available power is assumed constant, recall that $P_{max} = P_{ref}$. Applying the necessary conditions of the Euler-Lagrange theorem reveals the following differential equations governing the co-states:

$$\dot{\boldsymbol{\lambda}} = -\left(\frac{\partial H}{\partial \boldsymbol{x}}\right)^T = \begin{bmatrix} -\lambda_{\boldsymbol{v}}^T \left(\frac{\partial f_n}{\partial \boldsymbol{r}}\right) \\ -\lambda_{\boldsymbol{r}}^T - \lambda_{\boldsymbol{v}}^T \left(\frac{\partial f_n}{\partial \boldsymbol{v}}\right) \\ \lambda_{\boldsymbol{v}} \frac{T}{m^2} \end{bmatrix} \tag{7}$$

under the assumption of a constant power level [27]. However, when the available power is modeled to vary with the distance of the spacecraft from the Sun, the maximum power is equal to $P_{max} = P_{ref}/d_1^2$. Under the assumption of a varying power level, the necessary conditions of the Euler-Lagrange theorem produce a slightly modified set of differential equations governing the co-states, written as

$$\dot{\boldsymbol{\lambda}} = -\left(\frac{\partial H}{\partial \boldsymbol{x}}\right)^T = \begin{bmatrix} -\boldsymbol{\lambda}_{\boldsymbol{v}}^T \left(\frac{\partial \boldsymbol{f}_n}{\partial \boldsymbol{r}}\right) + \lambda_m \frac{T^2}{P_{\text{ref}}} \boldsymbol{d}_1 \\ -\boldsymbol{\lambda}_{\boldsymbol{r}}^T - \boldsymbol{\lambda}_{\boldsymbol{v}}^T \left(\frac{\partial \boldsymbol{f}_n}{\partial \boldsymbol{v}}\right) \\ \lambda_{\boldsymbol{v}} \frac{T}{m^2} \end{bmatrix} \tag{8}$$

The additional term in the vector differential equation governing the position co-states reflects the dependence of the position vector of the spacecraft relative to the Sun on the configuration space variables [27]. When generating the arcs associated with a trajectory during the hybrid optimization process, the initial values of the co-states are appended to the initial state vector and simultaneously propagated forward in time using the system and co-state differential equations. Note, however, that to reduce the number of variables required to completely define a low-thrust-enabled arc, the initial mass co-state on the first low-thrust arc is set equal to unity without a loss of information [33].

B. Multiple Shooting Algorithm

Formulating a multiple shooting method begins with specifying a free variable vector describing a transfer that is discretized into a sequence of arcs. Consider an initial guess for a transfer composed of n total arcs, not including segments along the departure and arrival periodic orbits. Along the transfer, the type of arc is specified and held constant throughout the corrections process, with a total of n_C natural arcs and n_L arcs low-thrust arcs; object-oriented programming is used to encode whether the low-thrust engine is activated along each arc. First, two variables are used to enforce the boundary conditions: τ_D and τ_T, each representing the time between a specified fixed-point along the associated periodic orbit and the departure and arrival locations, respectively. Then, the i-th arc along the transfer is completely described by the vector $\boldsymbol{N}_i$. A free variable vector $\boldsymbol{X}$ describing a low-thrust transfer is then defined as

$$\boldsymbol{X} = [\tau_D, \boldsymbol{N}_1, \boldsymbol{N}_2, \ldots, \boldsymbol{N}_{n-1}, \boldsymbol{N}_n, \tau_T]^T \tag{9}$$

If the transfer is constructed for a VSI engine, the node at the beginning of the i-th arc is uniquely defined by the initial position and velocity vectors, mass, and co-state vector. The exception to this definition is the first arc, where the low-thrust engine is initially activated to enable the spacecraft to depart the starting periodic orbit. At the beginning of this first arc, the initial spacecraft mass is held constant and equal to the initial wet mass, while the mass co-state is fixed to equal unity; thus, these two quantities are not considered variables at the first node. Along an arc where a VSI engine is activated, the integration time is assumed to be constant and equal to a value specified during initial guess construction to ensure consistency with the optimization problem formulation. If the VSI engine is not activated along the i-th arc, neither the co-states nor the spacecraft mass are specified; however, the integration time Δt_i is included as a variable. Thus, the i-th node along a transfer constructed using a VSI engine is described by the following vector:

$$\boldsymbol{N}_i = \begin{cases} \left[\boldsymbol{s}_1^T, \boldsymbol{\lambda}_{\boldsymbol{r},1}^T, \boldsymbol{\lambda}_{\boldsymbol{v},1}^T\right] & \text{if } i = 1 \\ \left[\boldsymbol{x}_i^T, \boldsymbol{\lambda}_i^T\right] & \text{if } i > 1, \text{ low-thrust arc} \\ \left[\boldsymbol{s}_i^T, \Delta t_i\right] & \text{if } i > 1, \text{ natural arc} \end{cases} \tag{10}$$

for $i = [1, n]$ [34, 35]. For a transfer constructed using a VSI engine, $\boldsymbol{X}$ possesses a dimension of $(14+14(n_L-1)+7n_C)\times 1$.

The free variable vector for a transfer constructed using a CSI engine, however, is formulated slightly differently: the co-state vectors for the low-thrust arcs are replaced with the thrust direction unit vector $\boldsymbol{u}_i = u_{x,i}\hat{x} + u_{y,i}\hat{y} + u_{z,i}\hat{z}$ assumed to be constant along the arc in the rotating frame [6], the integration time along each low-thrust arc is allowed to vary, and a slack variable β_i is used to ensure the integration time along each arc is positive. Specifically, the i-th node along a transfer constructed using a CSI engine is described by the following vector:

$$\boldsymbol{N}_i = \begin{cases} \left[\boldsymbol{s}_1^T, \boldsymbol{u}_1^T, \Delta t_1, \beta_1\right] & \text{if } i = 1 \\ \left[\boldsymbol{x}_i^T, \boldsymbol{u}_i^T, \Delta t_i, \beta_i\right] & \text{if } i > 1, \text{ low-thrust arc} \\ \left[\boldsymbol{s}_i, \Delta t_i, \beta_i\right]^T & \text{if } i > 1, \text{ natural arc} \end{cases} \tag{11}$$

The resulting free variable vector for a CSI transfer possesses a dimension of $(13 + 12(n_L - 1) + 8n_C) \times 1$.

A constraint vector is defined to enforce the boundary conditions and continuity along the trajectory. First, boundary conditions are enforced using the expressions in Eq. (3); the initial spacecraft mass is considered fixed and does not require specification in the boundary conditions. Then, position and velocity continuity is enforced between all neighboring arcs along the transfer. Mathematically, this constraint is expressed in vector form between the end of the i-th arc and beginning of the $(i + 1)$-th arc as $\boldsymbol{F}_{s,i} = \left[\boldsymbol{s}_{i,f}^T - \boldsymbol{s}_{i+1}^T\right]$ where the subscript f represents a quantity propagated forward in time along the i-th arc for Δt_i. Then, if the VSI engine is activated along two neighboring arcs, denoted the i-th arc and $i + 1$-th arc, co-state continuity is enforced across these arcs using the vector constraint $\boldsymbol{F}_{VSI,\Lambda} = \left[\boldsymbol{\lambda}_{i,f}^T - \boldsymbol{\lambda}_{i+1}^T\right]$ for $\Lambda = [1, n_\ell]$ where n_ℓ is the number of neighboring low-thrust arc pairs. Mass continuity is enforced both between neighboring low-thrust arcs and between low-thrust arcs separated by coast arcs, written as $\Delta m_k = m_{i,f} - m_j$ for the i-th and j-th arcs with the VSI engine activated arcs where $k = [1, n_L - 1]$. Then, the complete constraint vector $\boldsymbol{F}(\boldsymbol{X})$ for a transfer constructed using a VSI engine is written as

$$\boldsymbol{F}(\boldsymbol{X}) = \left[\boldsymbol{s}_1^T - \boldsymbol{s}_D^T(\tau_D), \boldsymbol{F}_{s,1}, \ldots, \boldsymbol{F}_{s,n-1}, \boldsymbol{F}_{VSI,1}, \ldots, \boldsymbol{F}_{VSI,n_\ell-1}, \Delta m_1, \ldots, \Delta m_{n_L-1}, \boldsymbol{s}_{n,f}^T - \boldsymbol{s}_T^T(\tau_T)\right]^T \tag{12}$$

For a VSI transfer, this constraint vector possesses a dimension of $(11 + 6(n - 1) + 7(n_\ell - 1) + n_L) \times 1$.

To form the constraint vector for a transfer that leverages a CSI engine, recall that these transfers do not satisfy the optimality conditions; rather, the control strategy along a low-thrust arc is defined using the thrust direction unit vector, which is held constant along an arc in the rotating frame. If the CSI engine is activated along the i-th arc, a scalar constraint is used to ensure that the thrust direction is a unit vector, expressed mathematically as $U_i = u_{i,x}^2 + u_{i,y}^2 + u_{i,z}^2 - 1$. In addition, the variable integration time along the i-th arc is constrained to take on only positive values; the corresponding constraint is written as $TD_i = \Delta t_i - \beta_i^2$. Finally, if the low-thrust engine is activated along the i-th arc and the next low-thrust-enabled arc is the j-th arc, mass continuity is enforced via the Δm_k constraint. Using these definitions, the complete constraint vector for a transfer constructed with a CSI engine is written as

$$\boldsymbol{F}(\boldsymbol{X}) = \left[\boldsymbol{s}_1^T - \boldsymbol{s}_D^T(\tau_D), \boldsymbol{F}_{s,1}, \ldots, \boldsymbol{F}_{s,n-1}, TD_1, \ldots, TD_n, \Delta m_1, \ldots, \Delta m_{n_L-1}, U_1, \ldots, U_{n_L}, \boldsymbol{s}_{n,f}^T - \boldsymbol{s}_T^T(\tau_T)\right]^T \tag{13}$$

which possesses a dimension of $(14 + 7(n-1) + 2(n_L - 1)) \times 1$.

A low-thrust trajectory that satisfies the state continuity, optimality, and boundary conditions is recovered by iteratively adjusting the free variable vector until the constraint vector possesses a magnitude of zero, to within a tolerance of 1×10^{-12} nondimensional units [35, 36]. For an optimal trajectory, the initial guess is iteratively adjusted in either SNOPT or *fmincon*. For a nonoptimal transfer, Newton's method is used with a minimum norm solution and the matrix of partial derivatives of the constraint vector with respect to the free variables is formed using a combination of analytical expressions and numerically-approximated derivatives, calculated via a first-order forward difference [33, 34].

V. Results: Point Solutions in Engine Models of Increasing Fidelity

Locally optimal low-thrust **L:2-A:2-V:11** transfers from a Sun-Earth L_2 Lyapunov orbit to a 15.24° inclination L_2 vertical orbit are constructed for a SmallSat using various engine and power models. First, a locally optimal **L:2-A:2-V:11** continuous-thrust transfer is recovered for a constant power VSI engine in the low-thrust-enabled CR3BP using the initial guess in Fig. 2; the unconstrained and variable thrust magnitude for a constant power VSI engine offers the most flexibility in corrections. This solution is then used in a continuation-based approach to identify similar solutions for engine and power models of increasing fidelity. In the first continuation sequence, the continuous-thrust transfer for a constant power VSI engine is used to recover a similar transfer for a varying power VSI engine. In the second continuation sequence, the continuous-thrust transfer for a constant power VSI engine is used to define an initial guess for a transfer with coast arcs to support regular periods of scientific observations. The resulting solution is used as an initial guess for a transfer for a CSI engine; an engine model more reflective of current SmallSat technological capabilities. A roadmap of these two continuation sequences and the corresponding subsections is depicted in Fig. 3 for clarity. Through this continuation-based approach, locally optimal low-thrust transfers are recovered for various engine and power models in a more computationally-efficient manner than forming a new initial guess for each new model.

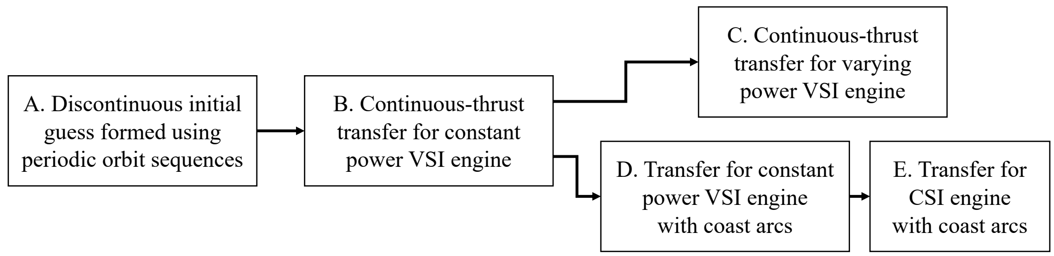

Fig. 3 Continuation sequences for recovering transfers in a variety of engine and power models.

A. Discretizing and Describing the Initial Guess

Discretization is required to convert a sequence of periodic orbits into an initial guess for use in a hybrid optimization scheme that leverages multiple shooting. For the **L:2-A:2-V:11** initial guess, displayed in Fig. 2, the Lyapunov, axial and vertical orbits are each discretized into eight arcs, evenly distributed in time. This discretization is selected to balance the sensitivity associated with corrections in the Sun-Earth L_2 region and the computational time required during optimization; of course, an alternative discretization scheme may produce a different locally optimal transfer. To construct the free variable vector for a continuous-thrust transfer with a constant power VSI engine, the states are sampled directly from the periodic orbit sequence, while the initial guess for each of the co-states is set to unity. The mass at the beginning of each low-thrust arc is then determined by multiplying the thrust duration by the mass flow rate, calculated from Eq. 2 using an estimate of the thrust and power from the co-states via Eqs. 6. Finally, initial guesses for τ_D and τ_T are set equal to the $1/8$ of the associated orbital period and measured from the x-axis crossing corresponding to a positive $\dot{y}$ velocity for the departure orbit and a positive $\dot{z}$ velocity for the arrival orbit, respectively. With this information, the discretized initial guess is summarized by $\boldsymbol{X}$, calculated via Eq. 9 and Eq. 10, and used to recover a continuous-thrust transfer for a constant power VSI engine. This initial guess may be iteratively adjusted if the corrections process fails to converge to a continuous solution, usually by scaling the initial co-state values.

B. Continuous-Thrust VSI Transfer

A continuous-thrust solution is identified for an **L:2-A:2-V:11** transfer to deliver a SmallSat from the selected Sun-Earth L_2 Lyapunov orbit to the target L_2 vertical orbit, assuming a VSI engine with a constant maximum power of 90 W. Applying the hybrid optimization scheme to the initial guess, the resulting continuous-thrust trajectory is displayed in Fig. 4 in (a) three-dimensional and (b) top-down views in the Sun-Earth rotating frame using dimensional coordinates. In this figure, the black, dashed arc represents the departure L_2 Lyapunov orbit, low-thrust arcs are depicted in red, and the target periodic orbit is indicated by a solid black arc. Inherited from the initial guess, this transfer consists of two segments with fundamentally different characteristics. In the first segment, the low-thrust engine significantly modifies the geometry of the path to connect to low amplitude vertical orbits via a small change in the inclination. For the locally-optimal transfer in Fig. 4, this first segment exhibits a noticeable deviation from the initial guess due to the

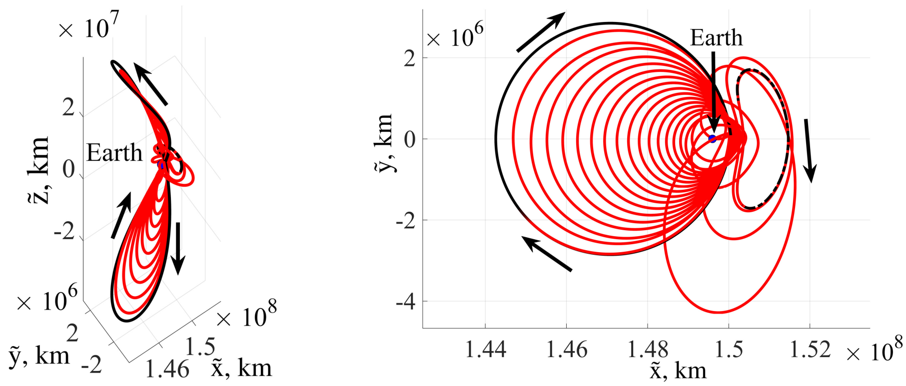

(a) Spatial view

(b) Projection onto the $xy-$ plane

Fig. 4 L:2-A:2-V:11 continuous-thrust transfer for a SmallSat with a constant power VSI engine.

sensitivity of correcting and optimizing a low-thrust-enabled arc that is seeded using a sequence of natural arcs with close passes to the Earth. The second segment of this transfer, however, closely resembles the geometry of members of the L_2 vertical family used to form the initial guess, producing a consistent increase in the inclination relative to the Sun-Earth plane. For an ESPA-class SmallSat, the recovered continuous-thrust trajectory for a constant power VSI engine requires a transfer time of 11.80 years and 43.26 kg of propellant; approximately 24% of the initial wet mass.

The thrust profile and the out-of-plane angle along the transfer offer further insight into the properties of the recovered solution as well as its utility as an initial guess to recover transfers with higher-fidelity power and engine models. The thrust magnitude profile for the entire transfer is displayed in Fig. 5(a) in red while the distance from the Earth is depicted in gray. During the second segment of the transfer, the thrust magnitude oscillates at a similar order of magnitude to the thrust level for the selected CSI engine, indicated by a black dashed line. However, during the first segment of the transfer, the thrust magnitude is consistently below 6 mN. This observation suggests that the recovered transfer, designed using a constant power VSI engine, may potentially supply a viable initial guess for use in a multiple shooting scheme to recover a transfer for the selected CSI engine; however, there may be some sensitivity during corrections, particularly along the first segment. Figure 5(b) depicts the thrust direction components in the velocity, normal, conormal (VNC) frame with respect to Earth, denoted u_v, u_n, and u_c, and depicted in blue, magenta, and maroon, respectively. In Figure 5(b), the thrust direction exhibits significant variation during the first segment; large changes in the thrust direction may be constrained according to operational requirements during subsequent analyses. However, during the second segment, the thrust direction only requires significant changes when the spacecraft is located at a locally-maximum distance from the Earth. For the remainder of this segment, the thrust direction is primarily aligned with the velocity vector relative to the Earth. Figure 6 depicts the out-of-plane (OOP) angle, measured from the Sun and with respect to the Sun-Earth plane. During the second segment of the trajectory, each year of thrusting increases the inclination by approximately 1°. In addition, the minima of the thrust magnitude profile generally coincide

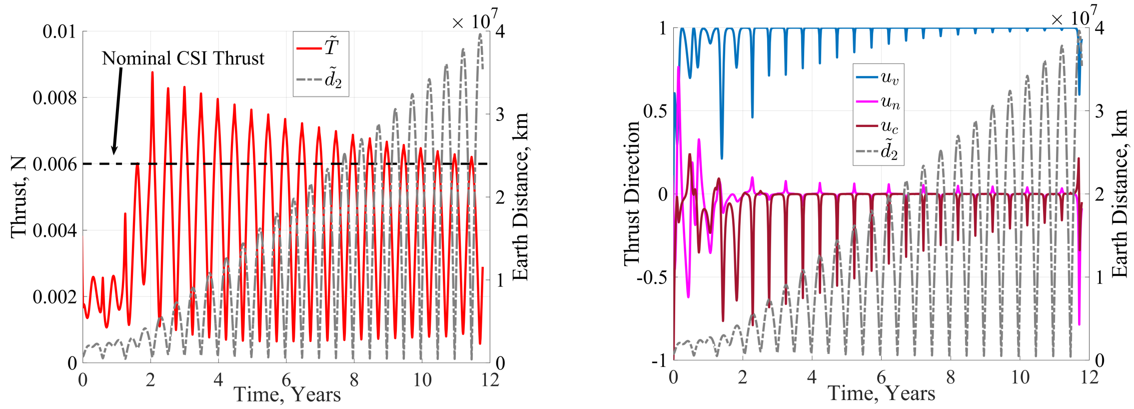

(a) Thrust magnitude profile

(b) Thrust directions

Fig. 5 Characteristics of L:2-A:2-V:11 continuous-thrust transfer for a constant power VSI engine.

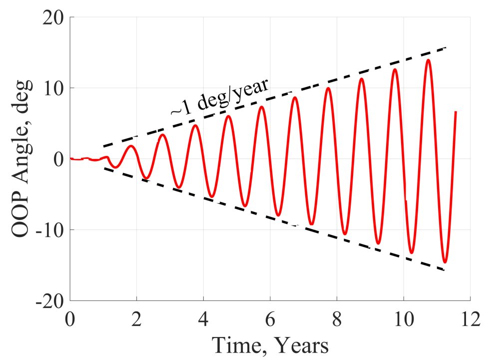

Fig. 6 Out-of-plane angle along a continuous thrust, constant power L:2-A:2-V:11 VSI transfer.

with the extrema of the out-of-plane angle along the trajectory. Accordingly, this continuous-thrust transfer is later modified to incorporate coast arcs near the extrema in the out-of-plane angle.

C. Continuous-Thrust VSI Transfer with Varying Power Levels

The continuous-thrust transfer designed with a constant power VSI engine is used as an initial guess for a transfer with a VSI engine and a model of the maximum available power that depends on the distance of the spacecraft from the Sun. Following hybrid optimization, the converged continuous-thrust **L:2-A:2-V:11** transfer for a varying power VSI engine appears in Fig. 7 with a configuration and color scheme consistent with Fig. 4(a), including (a) a three-dimensional view and (b) a projection onto the Sun-Earth plane. Along this transfer, the minimum distance from the Earth is 334,270 km; this quantity may be constrained and adjusted during subsequent analyses that incorporate higher-fidelity gravitational models and operational constraints. In addition, the flight time and propellant mass required are 11.80 years and 43.07 kg, respectively; similar to the properties of the transfer constructed for a constant power VSI engine. A comparison between Figs. 7 and 4 also reveals that the **L:2-A:2-V:11** transfers, each constructed using different power models, possess a similar geometry and characteristics. Figure 8(a) depicts the corresponding time history of the power,

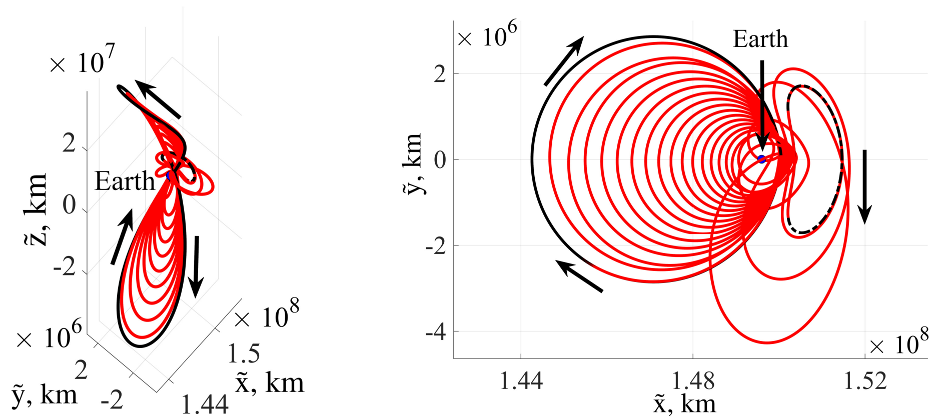

(a) Spatial view (b) Projection onto the $xy-$ plane

Fig. 7 L:2-A:2-V:11 continuous-thrust transfer for a SmallSat with a varying power VSI engine.

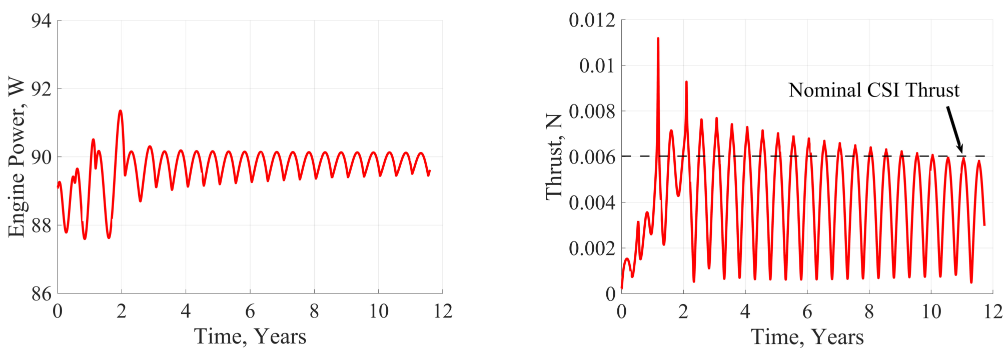

(a) Power profile (b) Thrust magnitude profile

Fig. 8 Characteristics of L:2-A:2-V:11 continuous-thrust transfer for a varying power VSI engine.

revealing oscillations throughout the transfer. The minima in the power occur when the spacecraft is well above and below the ecliptic plane, while the engine power increases above the nominal 90 W value when the distance of the spacecraft from the Sun is below 1 AU. Additionally, the thrust magnitude history along the transfer is displayed in Fig. 8(b) with the black dashed line representing the nominal thrust for the selected CSI engine, described in Table 1. Despite increasing the fidelity of the power model, the thrust magnitude profile for this transfer closely resembles that of the transfer constructed using a constant power VSI engine. Together, the similarity in the transfer geometry and thrust magnitude profile indicates that the solution constructed using the constant power assumption predicts the characteristics of a comparable transfer that exists in a higher fidelity power model for the VSI engine.

D. Constant Power VSI Transfer Integrating Coast Arcs

A **L:2-A:2-V:11** transfer that leverages both natural and low-thrust arcs is sought for a constant power VSI engine. Continuous activation of a low-thrust engine during a long transfer is not operationally feasible. Furthermore, in some cases, scientific instruments may not be able to operate with a sufficient accuracy while the engine is activated.

Thus, the continuous-thrust solution for a constant power VSI engine, displayed in Fig. 4, is used to construct an initial guess for a transfer for a fixed total thrust duration and incorporating coast arcs. Coast arcs are inserted into the vertical-like segments of the trajectory at locations where minimal thrust is required, i.e., centered around the extrema in the out-of-plane angle relative to the Sun. Placing the coast segments at these locations in the initial guess biases the optimization algorithm towards a solution that supports two scientific observational periods per year when the spacecraft is well above or below the Sun-Earth plane. Although these coast arcs are initially assumed to possess a duration of three months, they are allowed to vary in duration and location during corrections. Following hybrid optimization, the resulting trajectory, constructed for a VSI engine with constant power is displayed in Fig. 9 in the Sun-Earth rotating frame in dimensional coordinates via (a) a three-dimensional view and (b) a projection of the transfer onto the Sun-Earth plane. In these figures, the initial periodic orbit is represented by a black dotted arc, red depicts the low-thrust arcs, and black denotes the final periodic orbit. The coast segments are colored blue and possess a duration of approximately 3 months following optimization. Comparison of this trajectory to the solution in Fig. 4 reveals that the inclusion of coasting arcs to enable scientific observations does not significantly impact the transfer geometry. Similar to the continuous-thrust solution used to generate the initial guess, the transfer in Fig. 9 requires 44.69 kg of propellant, a flight time of 11.81 years, and passes as close as 395,440 km to the Earth. However, the thrust magnitude profile, displayed in Fig. 10 for the low-thrust segments along the transfer, is impacted by the inclusion of coasting periods along a transfer with a fixed total thrust duration. Although the general shape of the thrust magnitude history resembles that of the profile in Fig. 5(a) along arcs where the low-thrust engine is active, the mean thrust value has increased. The increase in thrust magnitude over a shorter total thrust duration requires the VSI engine to operate at a lower specific impulse, thereby increasing the required propellant mass. In subsequent analyses, selected coast arcs could be eliminated, particularly at lower inclinations, to reduce the required propellant mass while still prioritizing scientific observation periods at higher inclinations.

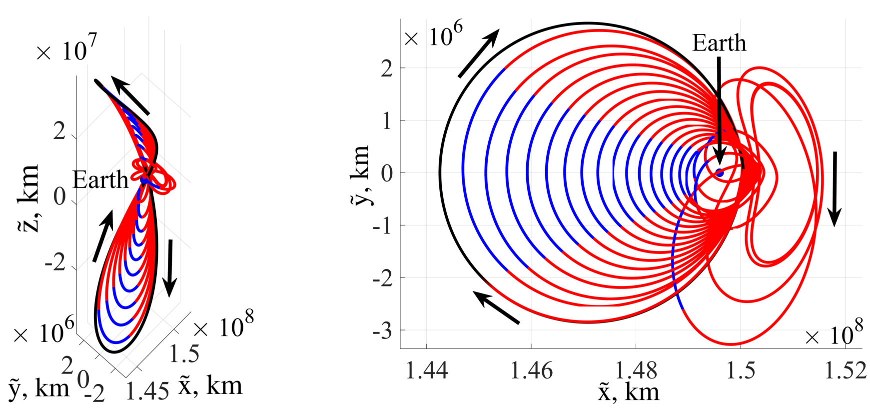

(a) Spatial view

(b) Projection onto the $xy-$ plane

Fig. 9 Constant power VSI L:2-A:2-V:11 transfer with thrust arcs in red and coast arcs in blue.

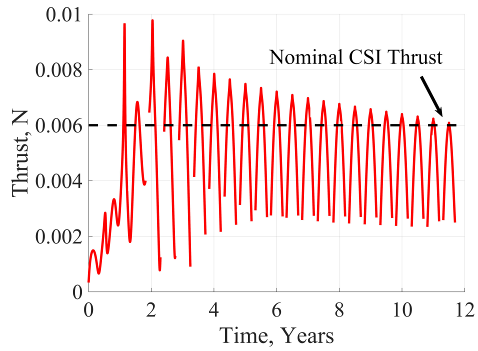

Fig. 10 Thrust magnitude along a constant power VSI L:2-A:2-V:11 transfer with thrust and coast arcs.

E. CSI Transfers

The **L:2-A:2-V:11** transfer with both natural and low-thrust arcs for a constant power VSI engine is used to recover a similar trajectory for a constant thrust, constant power CSI engine. The multiple shooting algorithm described in Section IV.B is used to produce a continuous transfer under the assumptions that the thrust magnitude is constant along low-thrust arcs and the thrust direction is fixed in the rotating frame along a single arc. Although the resulting solution is not locally optimal, the recovered trajectory tends to retain similar characteristics to the initial guess. Then, continuation is employed to gradually lower the propellant mass requirements by augmenting the constraint vector with an equality constraint on the spacecraft mass at the end of the final low-thrust arc along the transfer. To demonstrate this process, consider a SmallSat equipped with two JPL MiXI engines with a total thrust magnitude of 6 mN and a specific impulse of 3000 s, as summarized in Table 1. The trajectory displayed in Fig. 9 is then used to seed the initial guess under the same discretization scheme. However, a few low-thrust arcs with near-zero thrust values are replaced with coast arcs in the first segment of the transfer to reflect the higher thrust level of the MiXI engines. The free variable vector is then adjusted to use the node description scheme summarized in Eq. 11: co-states are replaced by a unit vector describing the thrust direction and integration times for the low-thrust arcs are also included. An initial guess for each unit vector is calculated using the average thrust direction in the Sun-Earth rotating frame over the corresponding low-thrust arc. The initial guess for the slack variables is straightforwardly derived as the square root of the integration time along each arc.

Following application of the multiple shooting algorithm to this initial guess, the resulting **L:2-A:2-V:11** transfer for the CSI engine is depicted in Fig. 11 with (a) a three-dimensional view and (b) a projection onto the Sun-Earth plane. In both figures, the color configuration is consistent with Fig. 9. Analysis of the trajectory in Fig. 11 reveals that this solution possesses a similar geometry to the initial guess. However, the centers of the coast arcs have shifted to impact the second segment of the trajectory. Such a result is expected given that the constant value of the thrust magnitude associated with the CSI engine is generally higher than the thrust magnitude along the majority of the locally optimal transfer associated with constant power VSI engine, as depicted in Fig. 5(a). Of course, alternate values of the thrust magnitude for a CSI engine may not produce the same results; in some cases, a similar solution may be difficult to

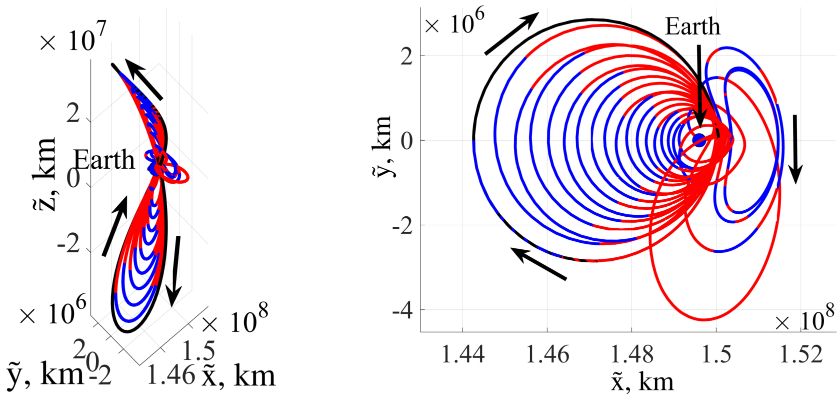

(a) Spatial view (b) xy-planar projection

Fig. 11 L:2-A:2-V:11 transfer with thrust and coast arcs for a SmallSat with a CSI engine.

recover or may not even exist. Nevertheless, the flight time for the transfer in Fig. 11 is 11.86 years while the required propellant mass and minimum approach distance to Earth are 49.43 kg and 409,530 km, respectively. Notably, the propellant mass usage has increased by approximately 5 kg relative to the initial guess due to significant changes in the thrust profile and the nonuniqueness of a solution recovered without local optimization.

Continuation in the final spacecraft mass is employed to identify a **L:2-A:2-V:11** transfer for the CSI engine with a lower required propellant mass. This continuation process is implemented by constraining the final spacecraft mass to a specified value and using multiple shooting to slightly adjust the solution as this value is gradually increased. This process repeats until the corrections algorithm cannot converge on a solution using the provided values of the thrust magnitude and specific impulse as well as the selected discretization. Using this approach, a transfer for the CSI engine is recovered with a lower required propellant mass of 47.5 kg. This transfer is displayed in Fig. 12 using (a) a three-dimensional view and (b) a projection onto the Sun-Earth plane. The flight time for this solution is 12.18 years while the minimum approach distance to Earth is 123,700 km. Of course, this perigee distance may be raised in subsequent analyses that use a higher-fidelity gravitational model and operational constraints. Comparison of this transfer to the initial guess in Fig. 11 reveals that the geometry and flight time have been modified to accommodate the 2 kg reduction in the required propellant mass. Specifically, the CSI transfer with a lower required propellant mass possesses a larger maximum apogee distance during the first segment of the transfer and longer coast arcs with an average of 3.66 months each during the second segment; simultaneously, the flight time increases by 3.84 months.

VI. Results: Exploring the Transfer Design Space

A preliminary exploration of the transfer design space is performed by recovering transfers for a constant power VSI engine from a variety of initial guesses. As demonstrated in the previous section, the solutions constructed for a constant power VSI engine offer an initial estimate of the characteristics of similar transfers associated with higher

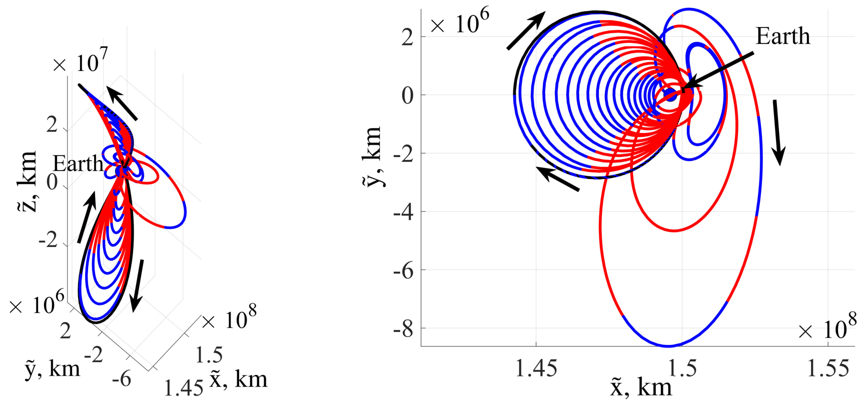

(a) Spatial view

(b) Projection onto the $xy-$ plane

Fig. 12 Lower propellant mass L:2-A:2-V:11 transfer with thrust and coast arcs for a CSI engine.

fidelity power and engine models. Thus, a preliminary exploration offers a rapid approximation of the flight time and required propellant mass; two metrics that are often used during mission and concept development. To begin the design space exploration, a set of initial guesses is constructed using distinct sequences of periodic orbits near Sun-Earth L_2. By varying the number and distribution of orbits sampled along each family, 43 initial guesses are assembled with each initial guess constrained to include at most three Lyapunov orbits, five axial orbits, and twelve vertical orbits. Each initial guess is used to recover a locally optimal continuous-thrust transfer for a VSI engine with constant power. As an example of these solutions, Figs. 13(a) and 13(b) portray **L:1-A:2-V:6** and **L:2-A:2-V:8** transfers for a constant power VSI engine. These transfers possess distinct geometries and characteristics from the **L:2-A:2-V:11** transfer displayed in Fig. 4, requiring flight times of 6.25 years and 8.84 years, respectively, and propellant masses of 73.74 kg and 53.39 kg. Several of the continuous-thrust solutions for a constant power VSI engine are used to identify similar transfers that incorporate coast arcs at locations well above and below the Sun-Earth plane, producing an additional 12 transfers. The 12 constant power VSI transfers with integrated coast arcs span a wide variety of the geometries explored, supplying preliminary insights into the solution characteristics when introducing coast arcs.

The constructed set of transfers enable a preliminary exploration of the trade-off between the required flight time and final spacecraft mass. Figure 14(a) displays the relationship between the flight time and final spacecraft mass for all of the generated transfers that use a constant power VSI engine. Red markers indicate the properties of continuous-thrust transfers, blue markers correspond to transfers with coast arcs, and the black dashed line represents the initial wet mass of the spacecraft, i.e., 180 kg. Furthermore, grey dashed lines connect the continuous thrust transfers used as an initial guess to recover transfers with integrated coast arcs that possess a similar geometry. Analysis of this figure reveals, as expected, that the flight time and final spacecraft mass are inversely related: longer flight times generally correspond to lower propellant mass usage and higher deliverable mass fractions. However, this relationship is not exact; some transfers possess lower flight times and propellant mass usage than other nearby transfers, an artifact of the transfer

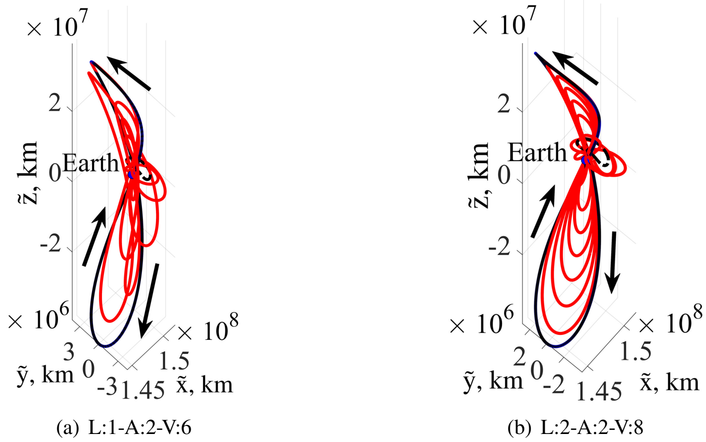

Fig. 13 Short and intermediate flight time transfers with a constant power VSI engine.

geometry of each initial guess and the associated local basins of convergence. In addition, the transfers with integrated coast arcs tend to possess nearly equivalent flight times compared to the continuous thrust transfers, but the final mass may be up to 10 kg lower. Nevertheless, there is a Pareto front characterizing the trade-off between final spacecraft mass and transfer duration. This front occurs significantly below the initial spacecraft mass and can be attributed to the large difference in energy between the initial orbit and final orbit. Across the set of recovered transfers, the solution with the lowest flight time requires approximately 4.88 years and requires a propellant mass of 117.22 kg. As the time required to reach the target 15.24° inclination L_2 vertical orbit increases across the recovered portion of the solution space, the propellant mass required for the SmallSat to complete this low-thrust transfer approaches a minimum value of approximately 40 kg. Figure 14(b) then depicts the flight time and final mass relationship for all of the constant power VSI transfers, but with the markers shaded by the number of vertical orbits used to construct the initial guess for the transfer. Analysis of this figure reveals that increases in flight time tend to be driven by the number of vertical orbits used to seed the initial guess. Together, these results support a rapid and preliminary exploration of the transfer design space

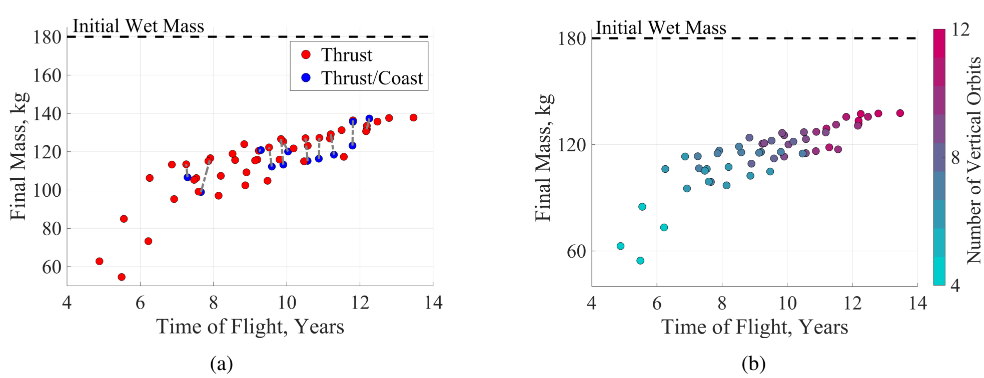

Fig. 14 Final spacecraft mass and flight time for constant power VSI transfers with varying geometries.

for a low-thrust-enabled SmallSat to reach a high-inclination orbit near Sun-Earth L_2. This analysis may be extended in future work to: examine the existence and properties of transfers that are seeded with initial guesses constructed using arcs along alternative dynamical structures such as nearby spatial stable and unstable manifolds or quasi-periodic trajectories, examine changes in the solution space for alternative combinations of initial and final orbits, incorporate constraints that bound the transfer design space, and recover similar solutions in more complex dynamical models.

VII. Conclusion

In this paper, low-thrust transfers are designed to reach highly out-of-ecliptic orbits to enable scientific investigations of interest to the heliophysics and astronomy communities. These transfers enable a SmallSat to reach a Sun-Earth L_2 vertical orbit with an inclination of 15.24° relative to the Sun-Earth plane from an L_2 Lyapunov orbit. An initial guess for each transfer is seeded using a sequence of periodic orbits from the L_2 Lyapunov, axial, and vertical orbit families in the circular restricted three-body problem (CR3BP), thereby exploiting the underlying dynamics of the Sun-Earth system. Each initial guess is input to a hybrid optimization scheme to recover a trajectory that maximizes the final spacecraft mass in a low-thrust-enabled CR3BP. This hybrid optimization scheme combines the optimality conditions derived from the Euler-Lagrange theorem with a multiple shooting algorithm to recover a locally optimal trajectory. This approach is used to study both the characteristics of a specific transfer type in engine and power models of increasing fidelity and the solution space encompassed by transfers of distinct geometries.

The characteristics of a point solution are examined across a variety of engine and power models: Variable Specific Impulse (VSI) and Constant Specific Impulse (CSI) engines, constant and varying power models, and continuous-thrust transfers and trajectories that incorporate both natural and low-thrust motion. The initial guess for this trajectory, labeled a **L:2-A:2-V:11** transfer, is constructed using two Lyapunov orbits, two axial orbits, and 11 vertical orbits. This initial guess is input to the hybrid optimization scheme to recover a continuous-thrust transfer for a constant power VSI engine that requires a flight time of 11.80 years and 43.26 kg of propellant for a SmallSat with an initial wet mass of 180 kg. This locally optimal solution is then used in two continuation sequences to recover the following types of transfers: a continuous-thrust transfer for a varying power VSI engine, a transfer for a constant power engine that incorporates both thrust and coast arcs, and a transfer for a CSI engine with both thrust and coast arcs. For the latter two transfer cases, regular coast arcs are placed well above and below the ecliptic plane, enabling the spacecraft to perform scientific observations in-transit approximately twice every year at increasing inclinations relative to the Sun-Earth plane. Through this continuation process, the transfers tend to possess a geometry and characteristics similar to that of the continuous-thrust transfer for a constant power VSI engine with the flight time and propellant mass increasing by only 139 days and 4.24 kg, respectively. As a result, transfers constructed for a constant power VSI engine appear to offer a useful mechanism for rapidly predicting whether a feasible trajectory may exist for a SmallSat to reach a high-inclination orbit and estimating its associated properties prior to higher-fidelity analyses.

A preliminary exploration of the transfer design space is conducted by selecting distinct sequences of baseline periodic orbits to seed multiple initial guesses. In this analysis, 43 continuous-thrust and locally optimal transfers of distinct geometries are constructed using a constant power VSI engine; 12 of these transfers are used to recover similar solutions with coast arcs when the spacecraft is well above and below the Sun-Earth plane. This solution space is composed of trajectories with flight times ranging from 4.8 to 13.5 years and requiring propellant masses between 40 kg and 125 kg, respectively, for an initial spacecraft mass of 180 kg. As expected, a higher final spacecraft mass generally corresponds to a higher flight time. This higher flight time is closely correlated with the number of vertical orbits used to construct the initial guess. Together, these transfers offer preliminary insight into the complex solution space, thereby supporting the trades that often occur during mission concept development: between the time to reach a target mission orbit, required propellant mass, and opportunities for scientific observations in transit during coast segments.

VIII. Acknowledgment

This research was carried out at the Jet Propulsion Laboratory, California Institute of Technology, under a contract with the National Aeronautics and Space Administration. Government sponsorship acknowledged.

References

[1] May, B. H., "A Survey of Radial Velocities in the Zodiacal Dust Cloud," Ph.D. Dissertation, Department of Physics, Imperial College, London, 2007. https://doi.org/10.1007/978-0-387-77706-1.

[2] Reach, W. T., Franz, B. A., and Weiland, J. L., "The Three-Dimensional Structure of the Zodiacal Dust Bands," *Icarus*, Vol. 127, 1997, pp. 461–484. https://doi.org/10.1006/icar.1997.5704.

[3] Wenzel, K., "The Ulysses Mission - A Voyage to the Poles of the Sun," *Nuclear Physics B - Proceedings Supplements*, Vol. 39, No. 1, 1995, pp. 59–68. https://doi.org/10.1016/0920-5632(95)00007-V.

[4] Pérez, J. M. S., "Trajectory Design of Solar Orbiter," *23rd International Symposium on Space Flight Dynamics, Pasadena, CA*, Vol. 17, 2012.

[5] Alibay, F., Bosanac, N., and Stuart, J. R., "A Low-Thrust-Enabled SmallSat Heliophysics Mission to Sun-Earth L5," *IEEE Aerospace Conference, Big Sky, MT*, 2018. https://doi.org/10.1109/AERO.2018.8396375.

[6] Elliott, I., Sullivan, C., Bosanac, N., Stuart, J. R., and Alibay, F., "Designing Low-Thrust Trajectories for a Small-Sat Mission to Sun-Earth L_5," *Journal of Guidance, Control and Dynamics*, Vol. 43, No. 10, 2020, pp. 1854–1864. https://doi.org/10.2514/1.G004993.

[7] Sullivan, C., Elliott, I., Bosanac, N., Alibay, F., and Stuart, J. R., "Exploring the Low-Thrust Trajectory Design Space for SmallSat Missions to the Sun-Earth Triangular Equilibrium Points," *29th AAS/AIAA Space Flight Mechanics Meeting, Ka'anapali, HI*, 2019.

[8] *CubeSat Design Specification*, California Polytechnic State University, 13th ed., February 2014.

[9] Whiffen, G. J., "Static/Dynamic Control for Optimizing a Useful Objective," , December 17 2002. U. S. Patent 6,496,741.

[10] Whiffen, G. J., "An Investigation of a Jupiter Galilean Moon Orbiter Trajectory," *AAS/AIAA Astrodynamics Specialist Conference, Big Sky, MT*, 2003.

[11] Whiffen, G., "Mystic: Implementation of the static dynamic optimal control algorithm for high-fidelity, low-thrust trajectory design," *AIAA/AAS Astrodynamics Specialist Conference and Exhibit, Keystone, CO*, 2006. https://doi.org/10.2514/6.2006-6741.

[12] Lo, M. W., "The Interplanetary Superhighway and the Origins Program," *Aerospace Conference Proceedings*, Vol. 7, IEEE, Big Sky, MT, 2002, pp. 3543–3562. https://doi.org/10.1109/AERO.2002.1035332.

[13] Anderson, R. L., and Lo, M. W., "Role of Invariant Manifolds in Low-Thrust Trajectory Design," *Journal of Guidance, Control, and Dynamics*, Vol. 32, No. 6, 2009, pp. 1921–1930. https://doi.org/10.2514/1.37516.

[14] Parker, J. S., and Anderson, R. L., *Low-Energy Lunar Trajectory Design*, John Wiley and Sons, Hoboken, New Jersey, 2014, pp. 95–113. https://doi.org/10.1002/9781118855065.

[15] Pritchett, R. E., Zimovan, E. M., and Howell, K. C., "Impulsive and Low-Thrust Transfer Design between Stable and Nearly-Stable Periodic Orbits in the Restricted Problem," *28th AIAA/AAS Space Flight Mechanics Meeting, Kissimmee, FL*, 2018. https://doi.org/10.2514/6.2018-1690.

[16] Das-Stuart, A., Howell, K. C., and Folta, D., "Rapid Trajectory Design in Complex Environments Enabled by Reinforcement Learning and Graph Search Strategies," *Acta Astronautica*, Vol. 171, 2019, pp. 172–195. https://doi.org/10.1016/j.actaastro.2019.04.037.

[17] Volle, M., "Optimal Variable-Specific-Impulse Rendezvous Trajectories Between Halo Orbits," *International Symposium on Space Flight Dynamics, Kanazawa, JPN*, Japan Society for Aeronautical and Space Sciences and ISTS, 2006.

[18] Russell, R., "Primer Vector Theory Applied to Global Low-Thrust Trade Studies," *Journal of Guidance, Control, and Dynamics*, Vol. 30, No. 2, 2007, pp. 460–473. https://doi.org/10.2514/1.22984.

[19] Senent, J., Ocampo, C., and Capella, A., "Low-Thrust Variable-Specific-Impulse Transfers and Guidance to Unstable Periodic Orbits," *Journal of Guidance, Control, and Dynamics*, Vol. 28, No. 2, 2005, pp. 280–290. https://doi.org/10.2514/1.6398.

[20] Mingotti, G., Topputo, F., and Bernelli-Zazzera, F., "Combined Optimal Low-Thrust and Stable-Manifold Trajectories to the Earth-Moon Halo Orbits," *New Trends in Astrodynamics and Applications III*, Vol. 886, No. 2, 2007, pp. 100–112. https://doi.org/10.1063/1.2710047.

[21] Betts, J., "Survey of Numerical Methods for Trajectory Optimization," *Journal of Guidance, Control, and Dynamics*, Vol. 21, No. 2, 1998, pp. 193–207. https://doi.org/10.2514/2.4231.

[22] Bryson, A. E., Jr., and Ho, Y.-C., *Applied Optimal Control*, Blaisdell Publishing, Waltham, MA, 1969, pp. 47–50. https://doi.org/10.1201/9781315137667.

[23] Gill, P., Murray, W., and Saunders, M., "SNOPT: An SQP Algorithm for Large-Scale Constrained Optimization," *Society for Industrial and Applied Mathematics Review*, Vol. 47, No. 1, 2005, pp. 99–131. https://doi.org/10.1137/S0036144504446096.

[24] MATLAB Optimization Toolbox, "MATLAB Optimization Toolbox Version 8.2," , 2018. The MathWorks, Natick, MA, USA.

[25] Goebel, D., Brophy, J., Polk, J., Katz, I., and Anderson, J., "Variable Specific Impulse High Power Ion Thruster," *Joint Propulsion Conference, Tucson, AZ*, AIAA/ASME/SAE/ASEE, 2005.

[26] Glover, T. W., Diaz, F. R. C., Ilin, A. V., and Vondra, R., "Projected Lunar Cargo Capabilities of High-Power VASIMR Propulsion," *Proceedings of 30th International Electric Propulsion Conference*, Florence, ITA, 2007.

[27] Stuart, J. R., Howell, K. C., and Wilson, R. S., "Automated Design of Propellant-Optimal, End-to-End, Low-Thrust Trajectories for Trojan Asteroid Tours," *Journal of Spacecraft and Rockets*, Vol. 51, No. 5, 2014, pp. 1631–1647. https://doi.org/10.2514/1.A32748.

[28] Szebehely, V., *Theory of Orbits*, 1st ed., Academic Press, New Haven, CT, 1967, pp. 16–22. https://doi.org/10.1016/B978-0-12-395732-0.X5001-6.

[29] Vallado, D. A., and McClain, W. D., *Fundamentals of Astrodynamics and Applications*, 3rd ed., Microcosm Press / Springer, El Segundo, CA, 2007, pp. 1041–1042.

[30] Jet Propulsion Laboratory, Distributed Spacecraft Technology Website, 2019. Accessed: December 10, 2019.

[31] Sakai, T., "A Study of Variable Thrust, Variable Specific Impulse Trajectories for Solar System Exploration," Ph.D. Dissertation, School of Aerospace Engineering, Georgia Institute of Technology, Atlanta, GA, 2004.

[32] Grebow, D. J., "Generating Periodic Orbits in the Circular Restricted Three-Body Problem with Applications to Lunar South Pole Coverage," M.S. Thesis, School of Aeronautics and Astronautics, Purdue University, West Lafayette, IN, 2006.

[33] Stuart, J. R., "A Hybrid Systems Strategy for Automated Spacecraft Tour Design and Optimization," Ph.D. Dissertation, School of Aeronautics and Astronautics, Purdue University, West Lafayette, IN, 2014.

[34] Stuart, J. R., Ozimek, M. T., and Howell, K. C., "Optimal, Low-Thrust, Path-Constrained Transfers between Libration Point Orbits using Invariant Manifolds," *AIAA/AAS Astrodynamics Specialist Conference, Toronto, CAN*, 2010. https://doi.org/10.2514/6.2010-7831.

[35] Pavlak, T. A., "Trajectory Design and Orbit Maintenance Strategies in Multi-Body Dynamical Regimes," Ph.D. Dissertation, School of Aeronautics and Astronautics, Purdue University, West Lafayette, IN, 2013.

[36] Bosanac, N., "Leveraging Natural Dynamical Structures to Explore Multi-Body Systems," Ph.D. Dissertation, School of Aeronautics and Astronautics, Purdue University, West Lafayette, IN, 2016.